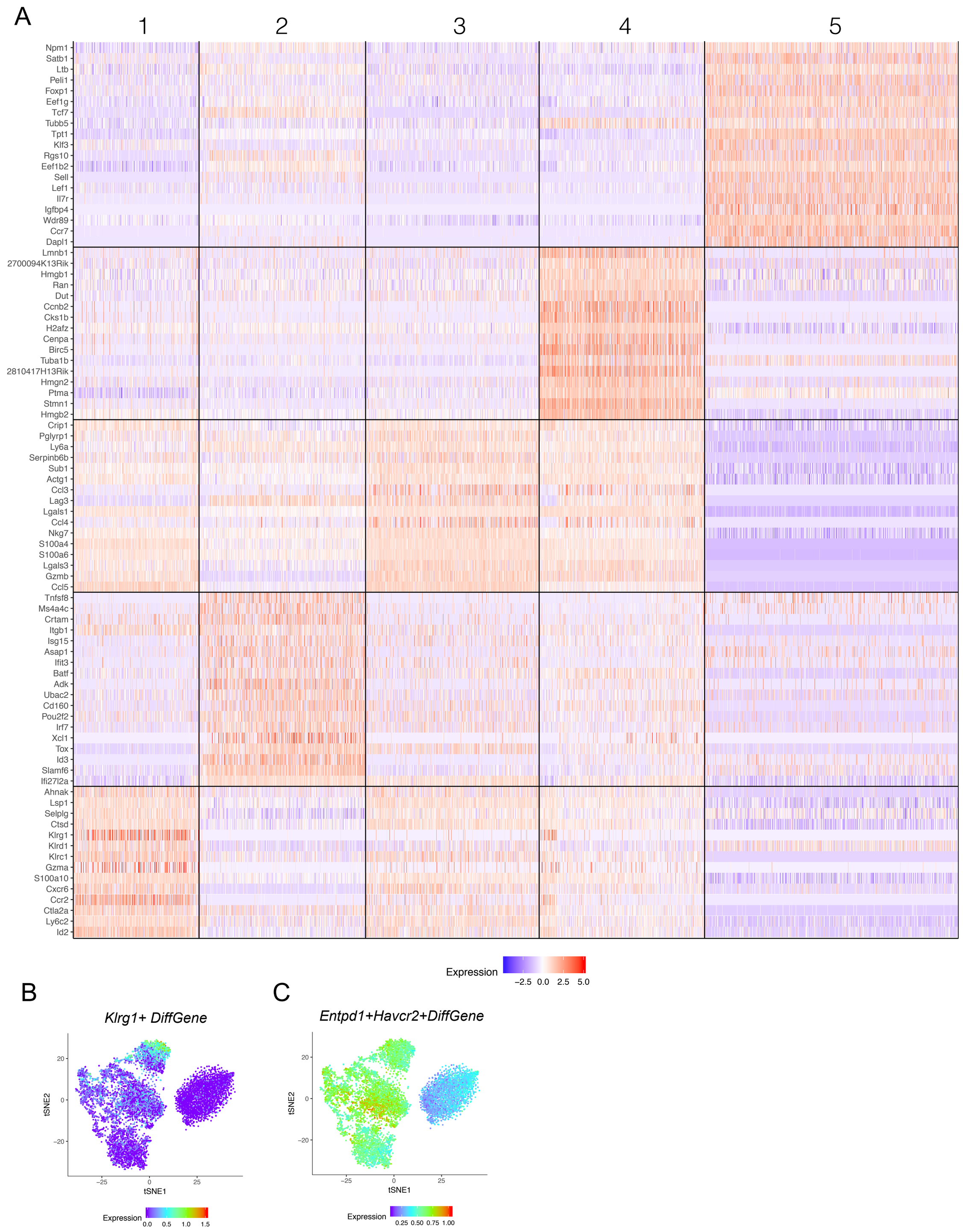

Figure S1. Significant differentially expressed genes across 5 scRNA-seq clusters.
*A.*Heatmap showing top 20 differentially expressed coding genes for the 5 clusters in **Figure 1B**.
B.Klrg1+ DiffGene signature in different clusters.
C.Entpd1+Havcr2+ DiffGene signature in different clusters.

Figure S1, Related to Figure 1

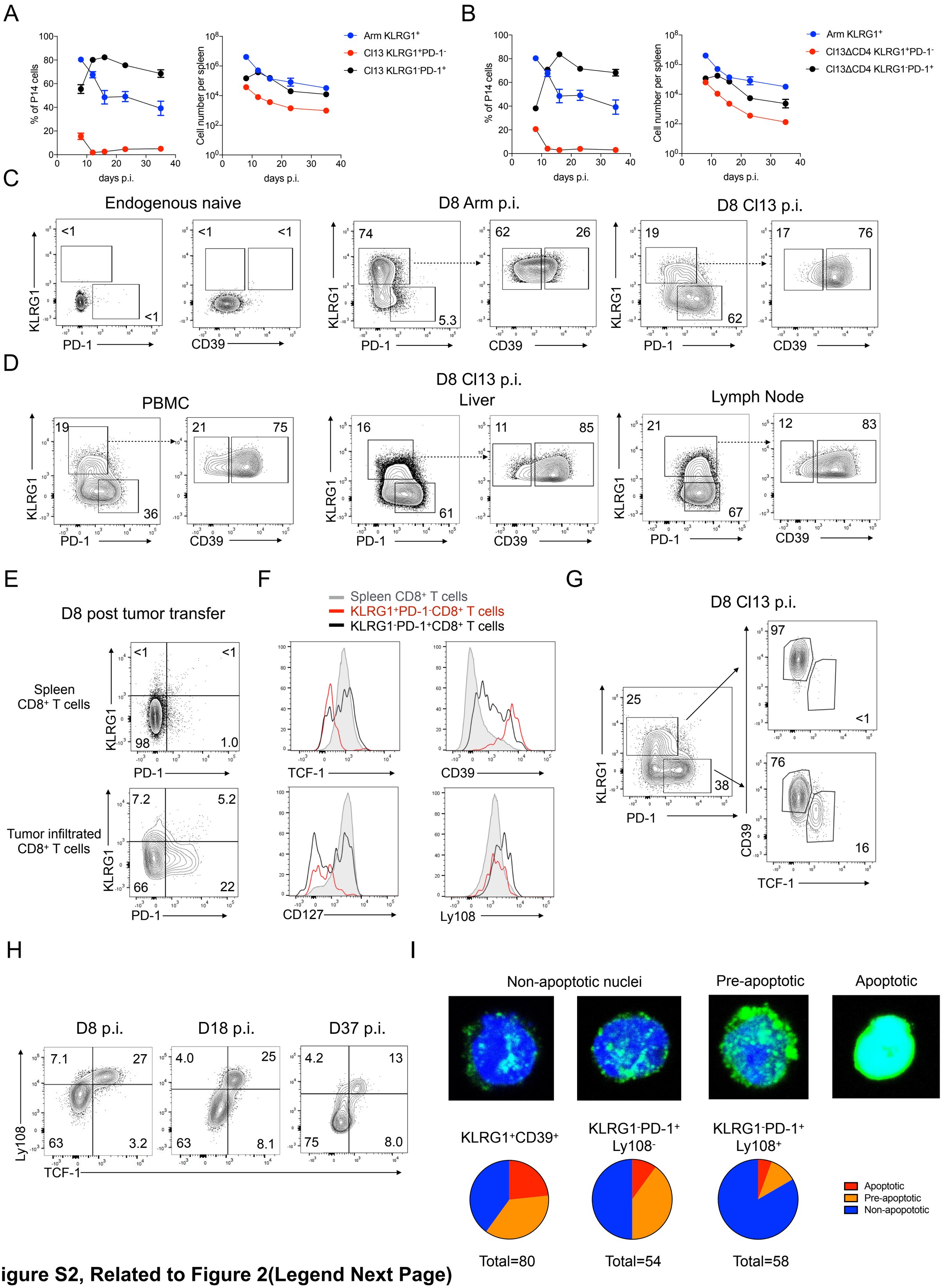

Figure S2, Related to Figure 2(Legend Next Page)

Figure S2. Population dynamics and molecular signatures of Teff-like and Tex precursor cells.

A. Population dynamics of KLRG1$^+$ P14 cells following LCMV Arm infection and KLRG1$^+$PD-1$^-$ or KLRG1$^-$PD-1$^+$ subsets of responding P14 cells during LCMV Cl13 infection.

B. Similar data as in part (**A**) for Cl13△CD4 infection. Note, the same LCMV Arm data from part (**A**) is plotted here for comparison.

C. KLRG1$^+$CD39$^+$ and KLRG1$^-$PD-1$^+$ P14 cells in spleens on D8 p.i. with Arm or Cl13. Gating strategies are based on staining of endogenous naïve cells. Plots are gated on donor P14 cells.

D. KLRG1 versus PD-1 as well as CD39 expression in KLRG1$^+$ responding P14 cells in the indicated tissues on D8 p.i. with Cl13. KLRG1$^+$ gate was based on staining of P14 cells in Arm infection and CD39$^-$ gate was based on staining of endogenous naïve cells.

E. Gating for KLRG1$^+$PD-1$^-$ and KLRG1$^-$PD-1$^+$ populations in the tumor infiltrating CD8 T cells (TILs) of CT26 tumor. Splenic CD8 T cells are shown as the gating control.

F. Phenotypic analysis of KLRG1$^+$PD-1$^-$ (red) and KLRG1$^-$PD-1$^+$ (black) TILs versus spleen CD8 T cells (green) on D8 post CT26 tumor inoculation. Representative KLRG1 versus PD-1 expression on TIL is shown in S2E.

G. Gating for KLRG1$^+$CD39$^+$TCF-1$^-$, KLRG1$^-$PD-1$^+$TCF-1$^-$ and KLRG1$^-$PD-1$^+$TCF-1$^+$ responding P14 cells at D8 p.i. with Cl13. The PD-1 versus KLRG1 gate was based on staining of endogenous CD44$^-$ naïve CD8 T cells.

H. Flow cytometry plots for co-expression of TCF-1 and Ly108 during Cl13 infection. The Ly108 versus TCF-1 gate was based on staining of endogenous CD8 T cells at each time point. Plots are gated on donor P14 cells.

I. Imaging of nuclear γH2AX staining. KLRG1$^+$CD39$^+$, KLRG1$^-$PD-1$^+$Ly108$^-$ and KLRG1$^-$PD-1$^+$Ly108$^+$ P14 CD8 T cells were sorted at D8 p.i. with Cl13 and stained with DAPI and for γH2AX.

Data are representative of 2-3 independent experiments with at least 3 mice/group.

Figure S2, Related to Figure 2

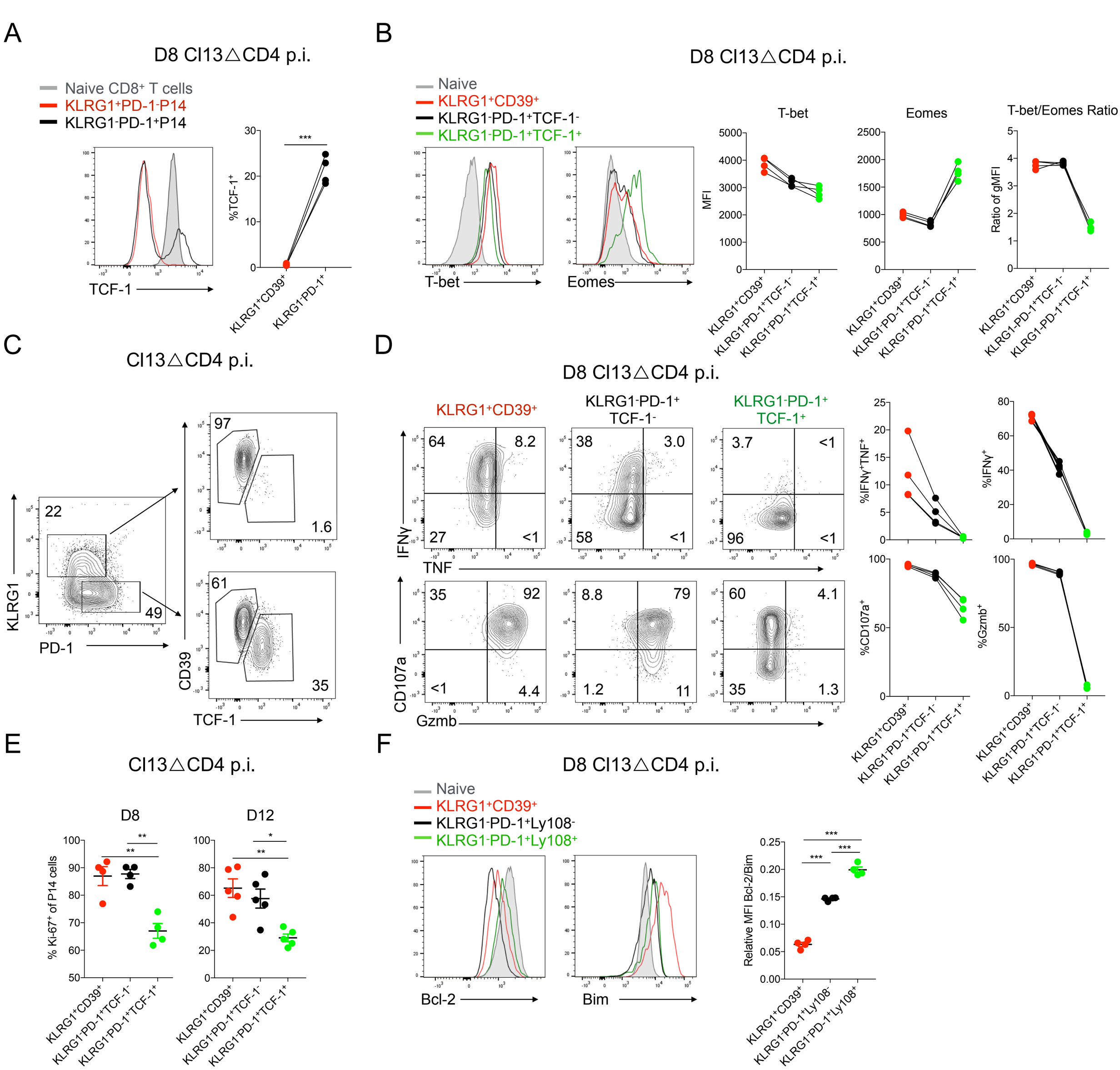

Figure S3. Identification of KLRG1$^+$CD39$^+$ Teff-like and PD-1$^+$TCF-1$^+$ Tex precursor cells in the absence of CD4 help.

A. TCF-1 expression in KLRG1$^+$CD39$^+$ and KLRG1$^-$PD-1$^+$ P14 cells at D8 of Cl13△CD4 infection. TCF-1 expression in endogenous naïve CD62L$^+$CD44$^-$CD8 T cells is shown as a control.

B. T-bet and Eomes expression in KLRG1$^+$CD39$^+$ and KLRG1$^-$PD-1$^+$ P14 cells at D8 of Cl13△CD4 infection. Naïve CD62L$^+$CD44$^-$CD8 T cells were again used as a control. T-bet/Eomes ratio was calculated based on geometric MFI.

C. Gating for KLRG1$^+$CD39$^+$TCF-1$^-$, KLRG1$^-$PD-1$^+$TCF-1$^-$ and KLRG1$^-$PD-1$^+$TCF-1$^+$ responding P14 cells at D8 of Cl13△CD4 infection. The PD-1 versus KLRG1 gate was based on staining of endogenous CD44$^-$ naïve CD8 T cells.

D. IFNγ, TNF, CD107a and Granzyme B (Gzmb) expression by KLRG1$^+$CD39$^+$ TCF-1$^-$, KLRG1$^-$PD-1$^+$TCF-1$^-$ and KLRG1$^-$PD-1$^+$TCF-1$^+$ subsets of responding P14 cells at D8 of Cl13△CD4 infection.

E. The percentage of Ki-67$^+$ cells in the KLRG1$^+$CD39$^+$, KLRG1$^-$PD-1$^+$TCF-1$^-$ or KLRG1$^-$PD-1$^+$TCF-1$^+$ subsets of P14 cells was assessed at D8 and D12 of Cl13△CD4 infection.

F. Bcl-2 and Bim expression were assessed at D8 p.i. of Cl13△CD4 infection in the KLRG1$^+$CD39$^+$, KLRG1$^-$PD-1$^+$Ly108$^-$ and KLRG1$^-$PD-1$^+$Ly108$^+$ subsets of P14 cells. Bcl-2 and Bim expression in naïve CD62L$^+$CD44$^-$CD8 T cells is shown as a control. The ratio of Bcl-2/Bim was calculated based on geometric MFI.

*P<0.05, **P<0.01, ***P<0.001 versus control (two-tailed Student's t-test and one-way Anova). Data are representative of 2 independent experiments with at least 4 mice/group (mean±s.e.m.).

Figure S3, Related to Figure 2

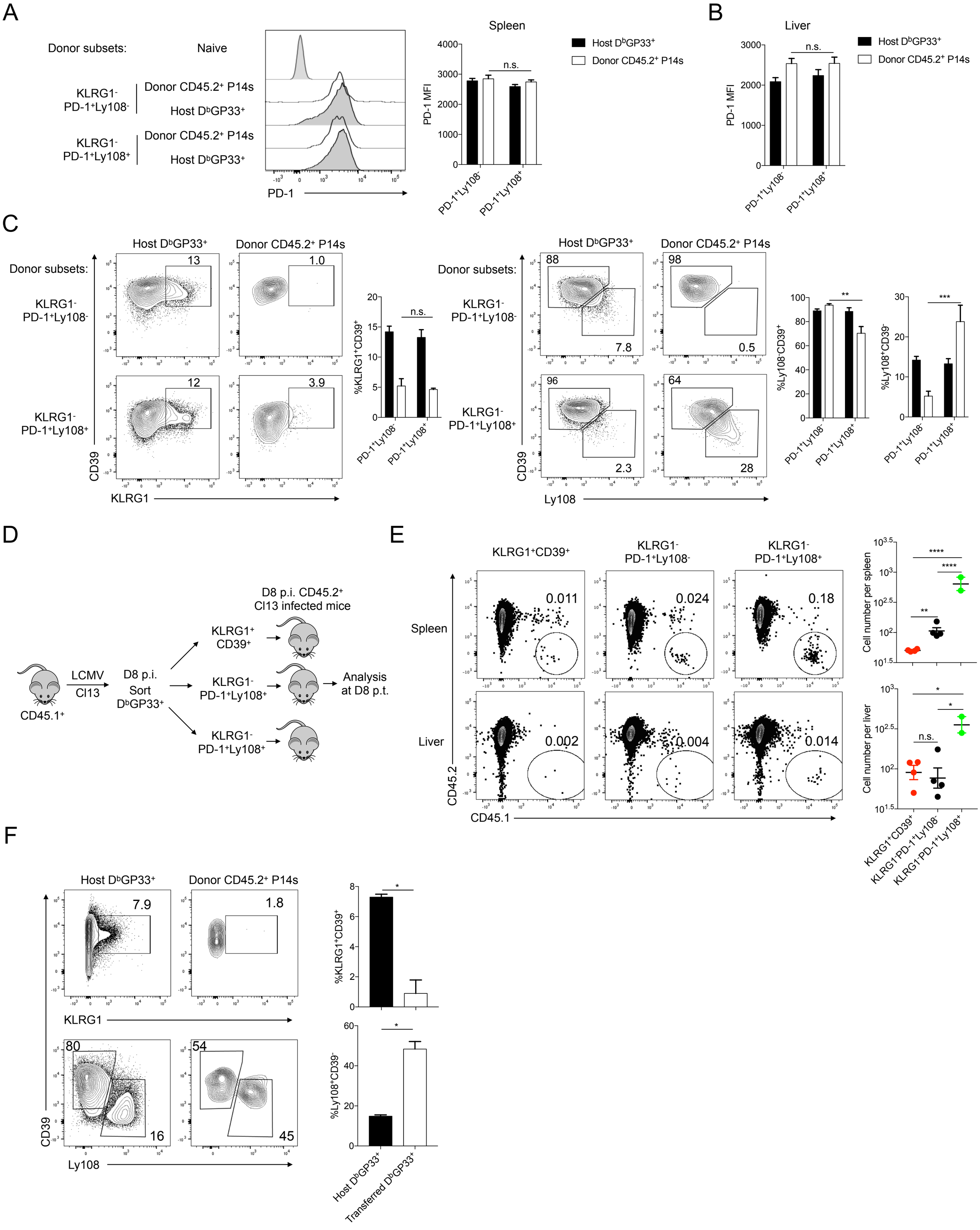

Figure S4, Related to Figure 3(Legend Next Page)

Figure S4. Lineage tracing for KLRG1^{+}CD39^{+} chronic Teff-like cells, KLRG1^{-}PD-1^{+}Ly108^{-} Tex cells and KLRG1^{-}PD-1^{+}Ly108^{+} Tex precursor cells.

A. Expression of PD-1 by CD45.2^{+} donor KLRG1^{-}PD-1^{+}Ly108^{-} or KLRG1^{-}PD-1^{+}Ly108^{+} P14 cells in the spleen following adoptive transfer into infection-matched recipient mice. Host D^{b}GP33 tetramer^{+} cells are shown as a control. Note, KLRG1^{+}CD39^{+} P14 cells isolated at D7 p.i. did not give rise to sufficient numbers of cells for analysis on D8 p.t. (see **Figure 3B**).

B. Expression of PD-1 by CD45.2^{+} donor KLRG1^{-}PD-1^{+}Ly108^{-} or KLRG1^{-}PD-1^{+}Ly108^{+} P14 cells in the liver following adoptive transfer into infection-matched recipient mice similar to part A. Note, KLRG1^{+}CD39^{+} P14 cells isolated at D7 p.i. did not give rise to sufficient numbers of cells for analysis on D8 p.t. (see **Figure 3B**).

C. Flow cytometry plots and quantification of CD45.2^{+} donor P14 cells and host D^{b}GP33 tetramer^{+} cells that are KLRG1^{+}, Ly108^{-}CD39^{+}, or Ly108^{+}CD39^{-} in the liver. Generation of each cell type is quantified for donor KLRG1^{-}PD-1^{+}Ly108^{-} and KLRG1^{-}PD-1^{+}Ly108^{+} subsets. Note, KLRG1^{+}CD39^{+} P14 cells isolated at D7 p.i. did not give rise to sufficient numbers of cells for analysis on D8 p.t. (see **Figure 3B**).

D. Experimental design. CD45.1^{+} mice were infected with Cl13. On D8 p.i. D^{b}GP33 tetramer^{+} CD8 T cells were sorted for KLRG1^{+}CD39^{+}, KLRG1^{-}PD-1^{+}Ly108^{-} or KLRG1^{-}PD-1^{+}Ly108^{+} subsets from the spleen. Equal numbers of each subset (1.7 x 10^{5} of each) were then adoptively transferred into infection matched (D8 p.i. Cl13) CD45.2^{+} recipient mice. Donor cells were analyzed on D8 p.t.

E. Flow cytometry plots and quantification of donor CD45.1^{+}CD8 T cells for the KLRG1^{+}CD39^{+}, KLRG1^{-}PD-1^{+}Ly108^{-} and KLRG1^{-}PD-1^{+}Ly108^{+} donor groups. Gated on D^{b}GP33^{+} CD8 T cells.

F. Flow cytometry plots and quantification of KLRG1^{+}CD39^{+}, Ly108^{-}CD39^{+} and Ly108^{+}CD39^{-} subsets of CD45.1^{+}CD8 T cells for the KLRG1^{-}PD-1^{+}Ly108^{+} donor cell group. Endogenous CD45.2^{+} D^{b}GP33^{+} CD8 T cells are used as gating controls.

**P*<0.05, ***P*<0.01, ****P*<0.001, *****P*<0.0001 versus control (two-tailed Student's *t*-test or One-Way ANOVA). The experiment has at least 2 mice/group (mean±s.e.m.).

Figure S4, Related to Figure 3

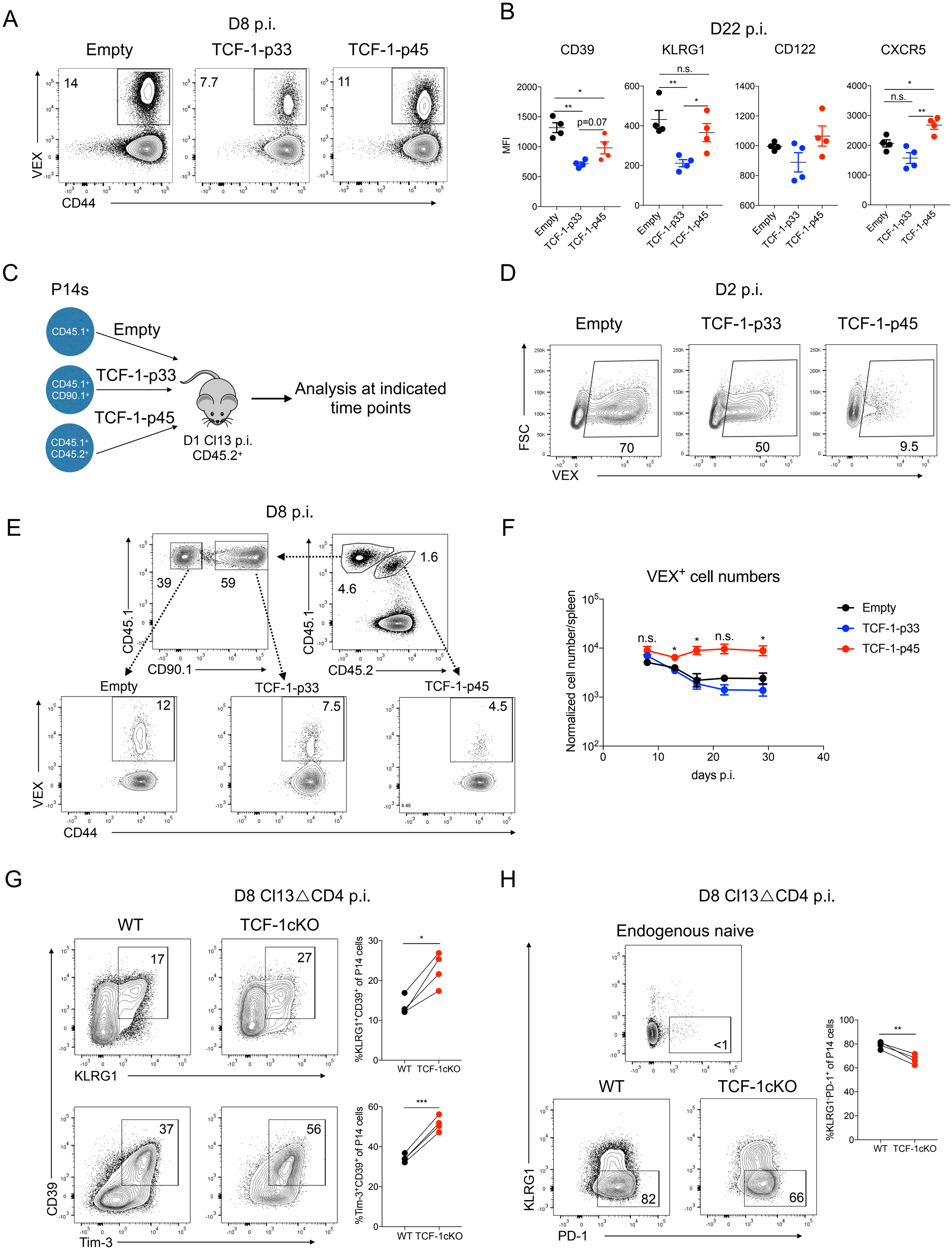

Figure S5, Related to Figure 4(Legend Next Page)

Figure S5. TCF-1 contributes to the development of Tex cells that persist.

A. Flow cytometry plots of P14 cells transduced with empty, TCF-1-p33 or TCF-1-p45 expressing RVs on D8 p.i. with Cl13. Gated on P14 cells.

B. CD39, KLRG1, CD122, CXCR5 expression on VEX^+ P14 cells transduced with Empty, TCF-1-p33 or TCF-1-p45 expressing RVs on D22 p.i. with Cl13.

C. Experimental design. WT P14 cells transduced with the indicated RVs were adoptively transferred to mice infected one day previously with Cl13. Donor RV transduced VEX^+ P14 cells were analyzed at the indicated time points.

D. VEX transduction efficiency on D2 p.i. for Empty-VEX, TCF-1-p33-VEX or TCF-1-p45-VEX RVs.

E. Gating for empty-VEX ($CD45.1^+CD45.2^-CD90.1^-VEX^+$), TCF-1-p33-VEX ($CD45.1^+CD45.2^-CD90.1^+VEX^+$) or TCF-1-p45-VEX($CD45.1^+CD45.2^+CD90.1^-VEX^+$) on D8 p.i.

F. VEX^+ P14 cell numbers were normalized to 1 X 10^4 VEX^+ P14 cell engraftment according to the transduction efficiency on D2 p.i. and analyzed at D8, D12, D16, D22, D30 Cl13 p.i.

G. Flow cytometry plots and quantification of $KLRG1^+CD39^+$ and $Tim\text{-}3^+CD39^+$ subsets of WT and TCF-1cKO responding P14 cells on D8 p.i. with Cl13.

H. Flow cytometry plots and quantification of the $KLRG1^-PD\text{-}1^+$ subset of WT and TCF-1cKO responding P14 CD8 T cells on D8 p.i. with Cl13. The PD-1 versus KLRG1 gate was based on staining of $CD44^-$ naïve CD8 T cells.

*P<0.05, **P<0.01, ***P<0.001 versus control (One-way Anova or two-tailed Student's t-test). Data are representative of 2 independent experiments with at least 4 mice/group (mean±s.e.m.).

Figure S5, Related to Figure 4

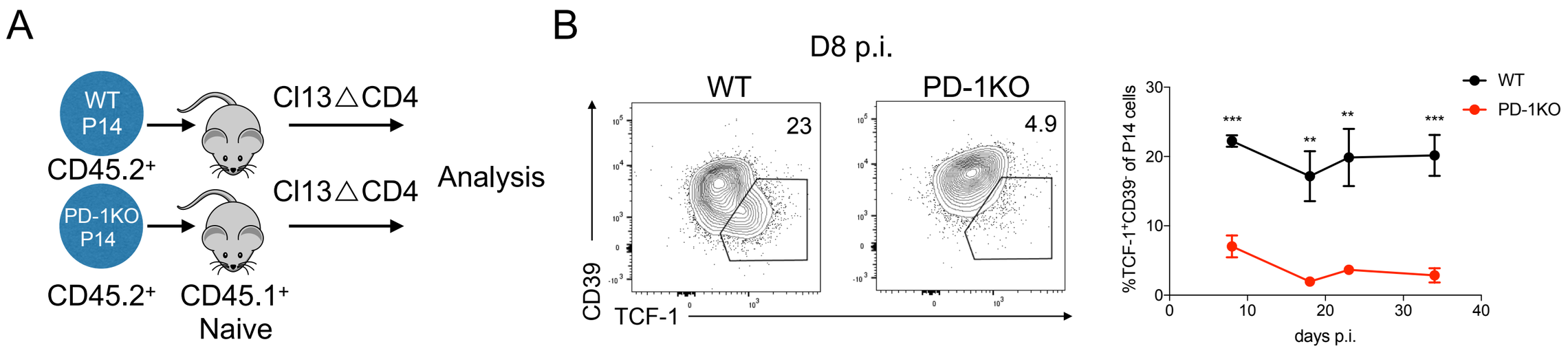

Figure S6. PD-1 sustains the TCF-1⁺ Tex cell precursor pool during chronic infection.

A. Experimental Design. 5 x 10^2 CD45.2⁺ WT P14 or 5 x 10^2 CD45.2⁺ PD-1KO P14 CD8 T cells were adoptively transferred into separate CD45.1⁺ naïve recipient mice and these recipients were treated with GK1.5 followed by infection with Cl13.

B. Flow cytometry plots to detect TCF-1⁺CD39⁻ P14 cells on D8 p.i. Summary analysis for the percent of donor TCF-1⁺CD39⁻ P14 cells present in the spleen on D8, D17, D22, D34 p.i. with Cl13 is shown.

**P*<0.05, ***P*<0.01, ****P*<0.01 versus control (two-tailed Student's *t*-test). Data represents 2 independent experiments (mean±s.e.m.) with at least 3 mice/group.

Figure S6, Related to Figure 5

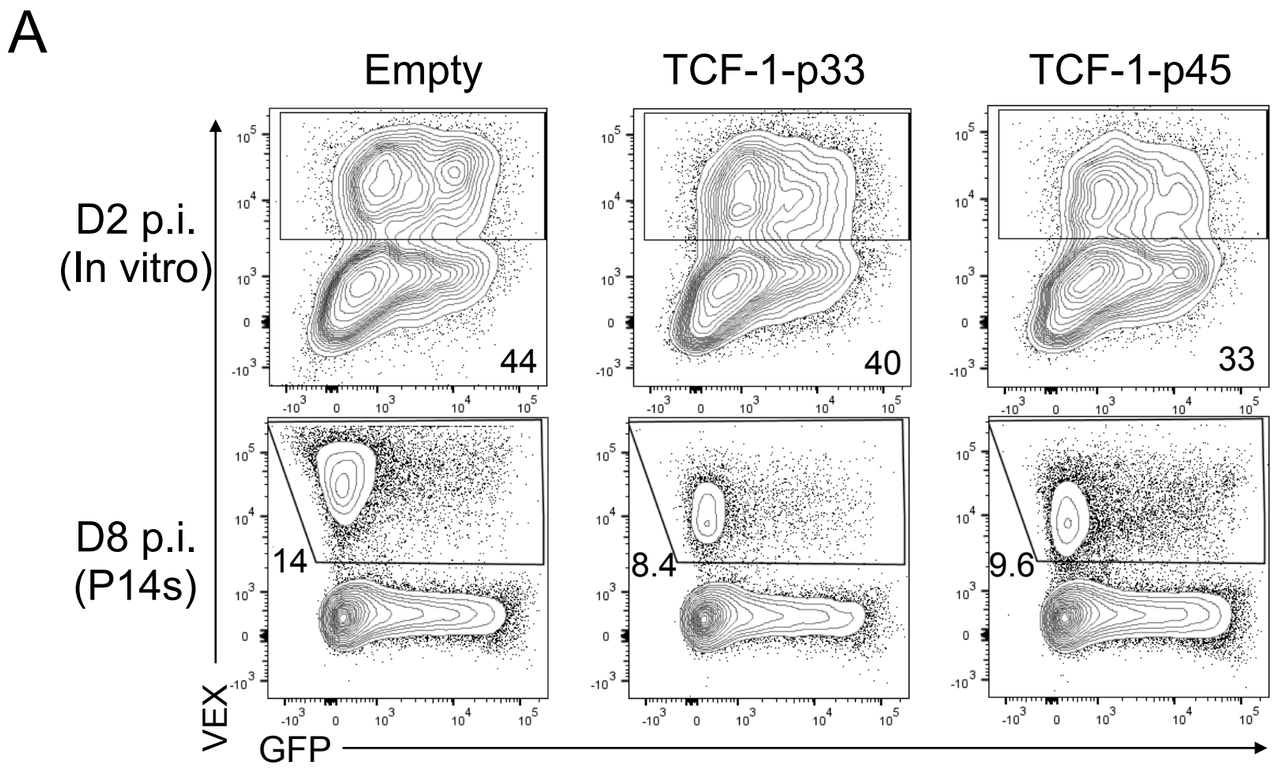

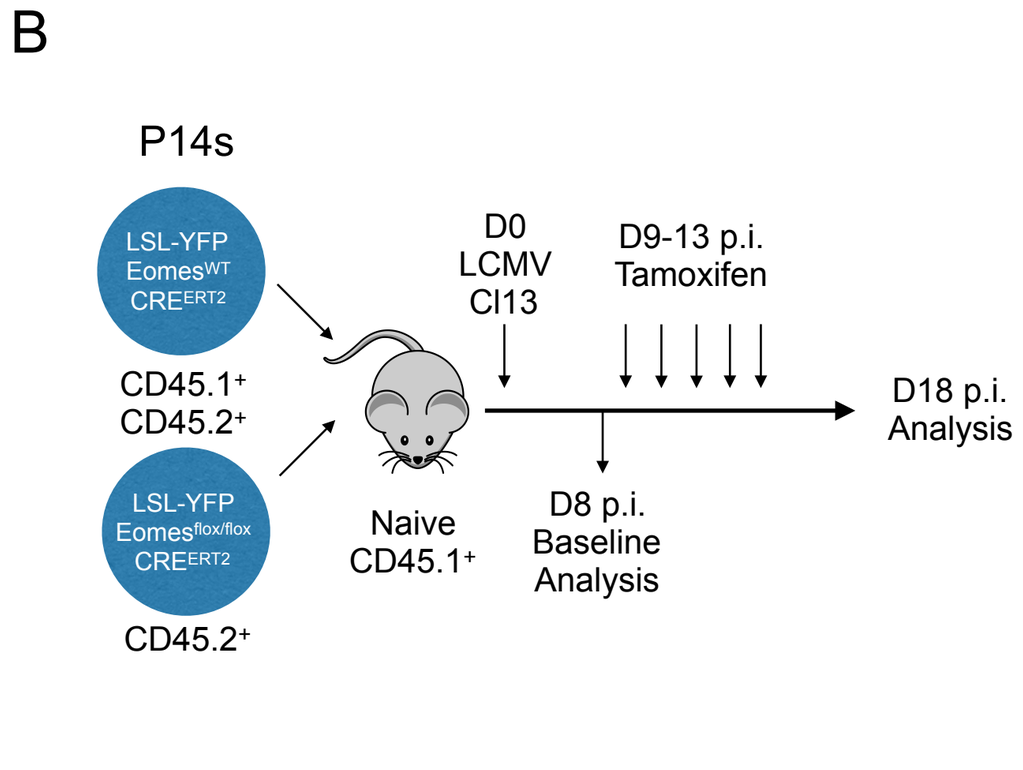

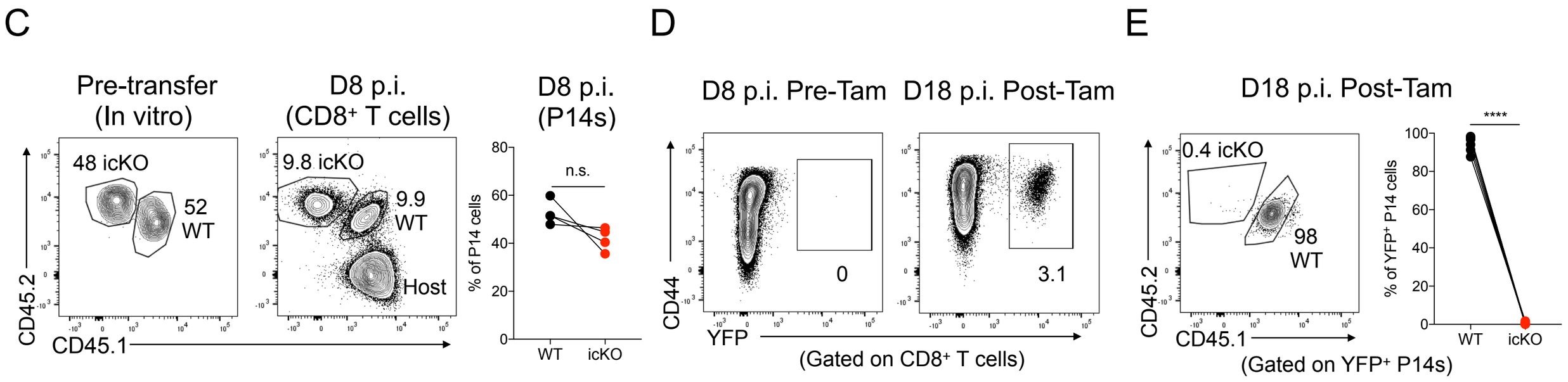

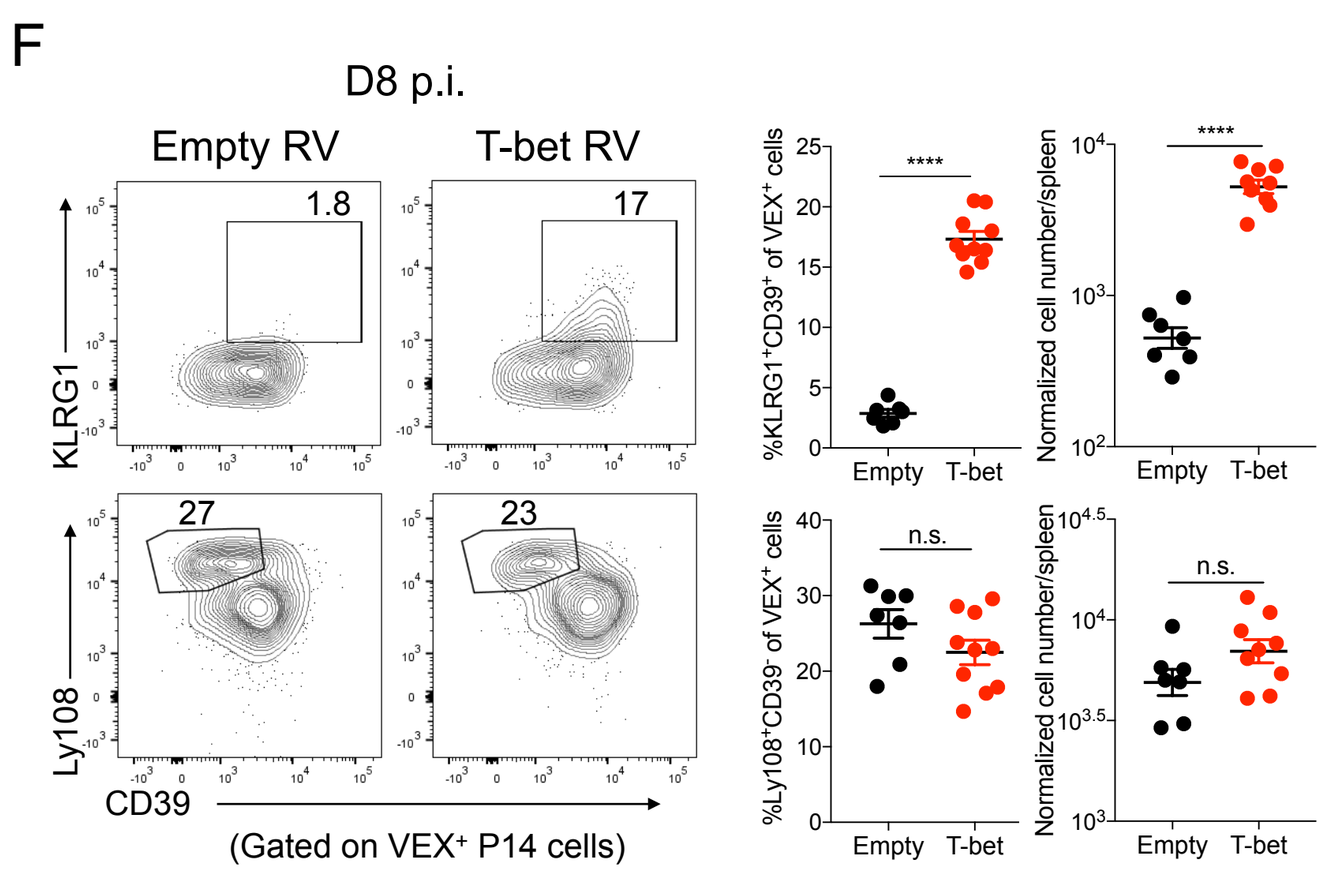

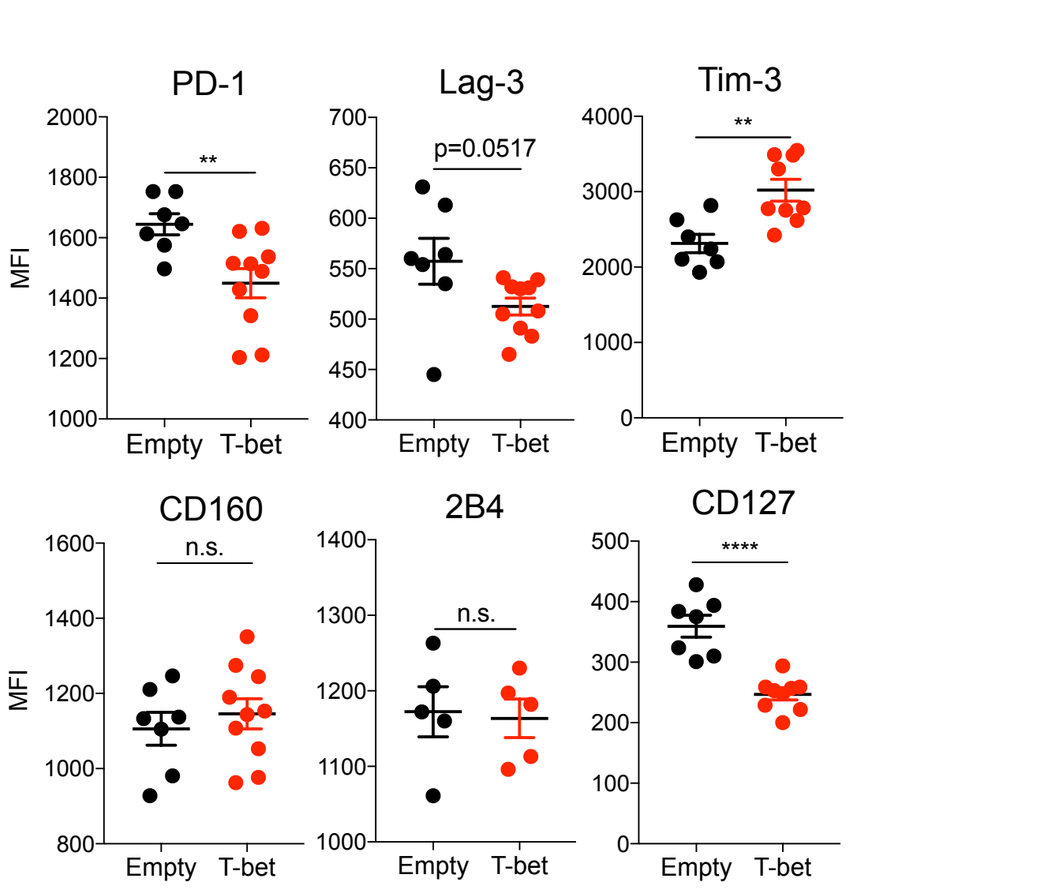

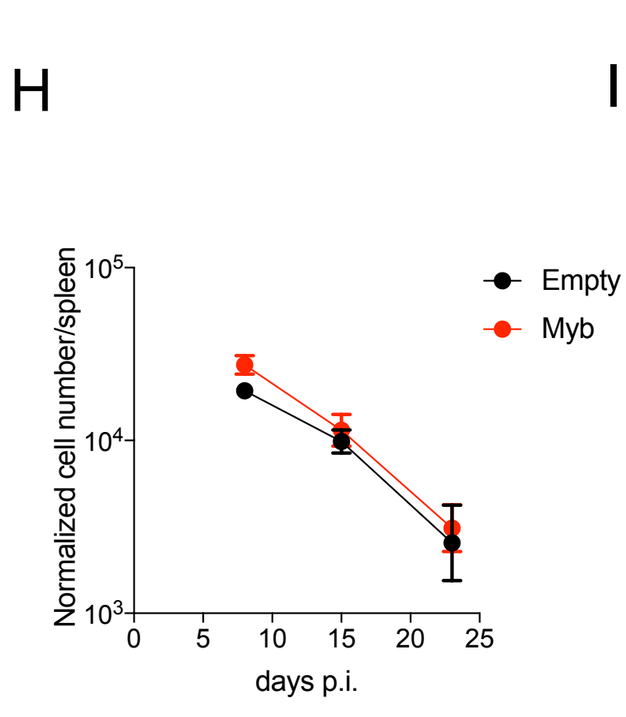

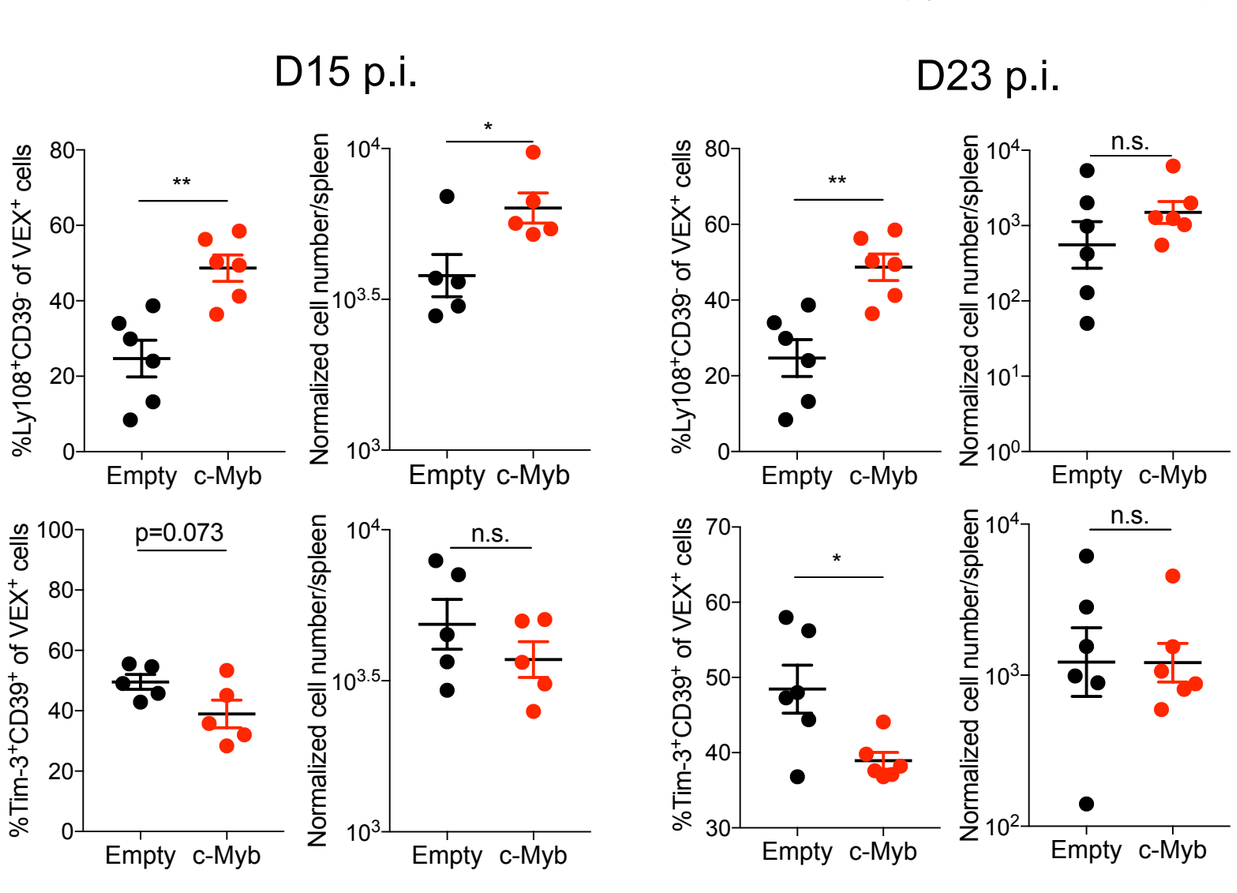

Figure S7, Related to Figure 7(Legend Next Page)

Figure S7. Effect of TCF-1-related TFs during Tex development.

A. Transduction of *Eomes*^{GFP} P14 cells with empty, TCF-1-p33, or TCF-1-p45 expressing RVs. Representative flow cytometry plots of P14 cells indicating transduction efficiency on D2 following transduction and on D8 p.i. with Cl13.

B. Experimental design. 2 x 10^3 CD45.2$^+$xRosa$^{LSL\text{-}YFP}$x*Eomes*$^{flox/flox}$xCRE^{ERT2} P14 cells and 2 x 10^3 CD45.1$^+$CD45.2$^+$x Rosa$^{LSL\text{-}YFP}$x*Eomes*^{WT}xCRE^{ERT2} control P14 cells were co-transferred into naive CD45.1$^+$ recipients and these recipient mice infected with Cl13. These recipient mice were then treated with tamoxifen from D9 p.i. to D13 p.i. At D18 p.i. donor YFP$^+$ (i.e. indicating CRE activity) P14 cells were analyzed.

C. Flow cytometry plots and quantification of pre-transfer P14 cell mix and D8 p.i. before tamoxifen treatment. Samples at D8 p.i. were collected from spleen.

D. Flow cytometry plots of pre (D8 p.i.) and post (D18 p.i.) tamoxifen treatment. Gated on CD8 T cells.

E. Flow cytometry plots and quantification of YFP$^+$ P14 cells after tamoxifen treatment (D18 p.i.).

F. Flow cytometry plots and quantification of KLRG1$^+$CD39$^+$ and Ly108$^+$CD39$^-$ subsets of responding P14 cells transduced with empty versus T-bet expressing RVs. Plots are gated on transduced (VEX$^+$) donor P14 cells on D8 p.i. with Cl13. Note: Empty controls are the same controls as Figure 7J.

G. Expression of PD-1, Lag-3, Tim-3, CD160, 2B4 and CD127 in the P14 cells transduced with empty versus T-bet RVs on D8 p.i. with Cl13.

H. Number of donor P14 cells transduced with empty versus c-Myb expressing RV at the indicated time points. VEX$^+$ cell numbers were normalized to 1 x 10^4 VEX$^+$P14 cell engraftment according to the transduction efficiency on D2 p.i. and analyzed at D8, D15 and D23 Cl13 p.i.

I. Quantification of Ly108$^+$CD39$^-$ and Tim-3$^+$CD39$^+$ subsets of responding P14 cells transduced with empty versus c-Myb RVs. Plots are gated on transduced (VEX$^+$) donor P14 cells on D15 and D23 p.i. with Cl13. VEX$^+$ cell numbers were normalized to 1 x 10^4 VEX$^+$ P14 cell engraftment according to the transduction efficiency on D2 p.i.

**P*<0.05, ***P*<0.01, ****P*<0.001, *****P*<0.001 versus control (two-tailed Student's *t*-test and One-Way Anova analysis). Data are representative of 2 independent experiments (mean±s.e.m.) with at least 3 mice/group.

Figure S7, Related to Figure 7